Loosely coherent search in LIGO O1 data for continuous gravitational waves from Terzan 5 and the Galactic Center

Vladimir Dergachev, Maria Alessandra Papa, Benjamin Steltner, and Heinz-Bernd Eggenstein

Phys. Rev. D **99**, 084048 — Published 30 April 2019

DOI: 10.1103/PhysRevD.99.084048

Loosely coherent search in LIGO O1 data for continuous gravitational waves from Terzan 5 and the galactic center

Vladimir Dergachev,[1,2,a] Maria Alessandra Papa,[1,2,b] Benjamin Steltner,[1,2,c] and Heinz-Bernd Eggenstein[1,2,d]

[1] *Max Planck Institute for Gravitational Physics (Albert Einstein Institute), Callinstrasse 38, 30167 Hannover, Germany*
[2] *Leibniz Universität Hannover, D-30167 Hannover, Germany*

We report results of a search for continuous gravitational waves from a region covering the globular cluster Terzan 5 and the galactic center. Continuous gravitational waves are expected from fast-spinning, slightly non-axisymmetric isolated neutron stars as well as more exotic objects. The regions that we target are believed to be unusually abundant in neutron stars. We use a new loosely coherent search method that allows to reach unprecedented levels of sensitivity for this type of search. The search covers the frequency band 475–1500 Hz and frequency time derivatives in the range of $[-3.0, +0.1] \times 10^{-8}$ Hz/s, which is a parameter range not explored before with the depth reached by this search. As to be expected with only a few months of data from the same observing run, it is very difficult to make a confident detection of a continuous signal over such a large parameter space. A list of parameter space points that passed all the thresholds of this search is provided. We follow-up the most significant outlier on the newly released O2 data and cannot confirm it. We provide upper limits on the gravitational wave strength of signals as a function of signal frequency.

I. INTRODUCTION

Continuous gravitational waves (CWs) are expected from fast-spinning neutron stars in a variety of circumstances, for example if they present a slight non-axisymmetry (ellipticity). Many CW searches have been carried out on LIGO data [1], including several all-sky searches [2–5] and broadband directed searches [6]. No signals have been detected yet.

Directed searches are searches for signals from interesting targets – both specific objects or/and regions. The search presented here, targeting emission from the globular cluster Terzan 5 and the galactic center, falls into this category.

We use data collected during the first Advanced LIGO observing run, O1, [7–10] and employ a new medium-scale loosely coherent algorithm [11–13]. We probe a broad class of signals with frequencies between 475 and 1500 Hz, with unprecedented sensitivity. For sources at 8.5 kpc this search is sensitive to signals from neutron star deformations well within the range allowed by conventional neutron star equations of state [14].

Additionally this search was used as a pilot study of the new loosely-coherent search method. The search uses a substantially longer coherence length than used before and hence presents most of the challenges and difficulties of an all-sky search, but without the substantial load of searching the whole sky. This search has exposed performance bottlenecks in the algorithms implementation and has paved the way for the first all-sky loosely coherent search [5].

The paper is organized as follows: sections II and III briefly introduce the LIGO detectors, the data that is used and the signal waveform that we target with this search. Section IV describes the features of the main building block of the search, the enhanced loosely coherent method, and section V illustrates the pipeline, including the way the upper limits are established and the ranking of the outliers. The results are presented and discussed in section VI. The appendix A contains the outlier tables.

II. LIGO INTERFEROMETERS AND THE O1 OBSERVING RUN

The LIGO gravitational wave detector consists of two 4 km dual-recycling Michelson interferometers, one in Hanford, Washington and the other in Livingston, Louisiana, separated by a 3000-km baseline. The interferometer mirrors act as test masses, and the passage of a gravitational wave induces a differential arm length change that is proportional to the gravitational-wave strain amplitude. The Advanced LIGO [9, 10] interferometers came online in September 2015 after a major upgrade.

The O1 run occurred between September 12, 2015 and January 19, 2016, from which approximately 77 days and 66 days of analyzable data were produced by the Hanford (H1) and Livingston (L1) interferometers, respectively.

Notable instrumental contaminants affecting the searches described here include spectral combs of narrow lines in both interferometers, many of which were identified after the run had ended and were mitigated for future runs [3, 4, 15]. For instance an 8-Hz comb in H1 with the even harmonics (16-Hz comb) being especially strong, was ascribed to digitization roundoff error in a high-frequency excitation applied in order to servo-control the cavity length of the Output Mode Cleaner

[a] vladimir.dergachev@aei.mpg.de
[b] maria.alessandra.papa@aei.mpg.de
[c] benjamin.steltner@aei.mpg.de
[d] heinz-bernd.eggenstein@aei.mpg.de

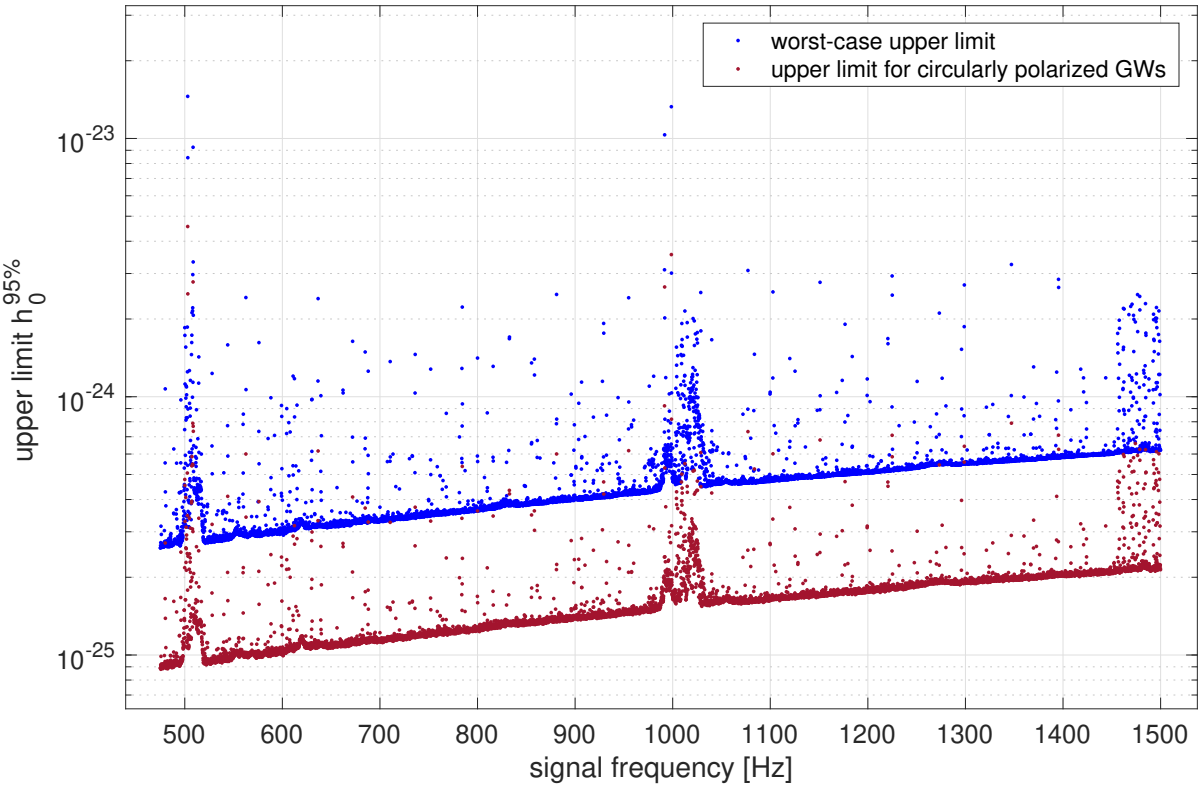

FIG. 1. Upper limits on gravitational wave strain. The dimensionless strain h_0 (vertical axis) is plotted against signal frequency. The upper (blue) curve shows worst-case (linearly polarized) 95% confidence level (CL) upper limits as a function of frequency. The upper limits are maximized over sky and all intrinsic signal parameters for each frequency band. The lower (red) curve shows upper limits assuming a circularly polarized source. The data for this plot can be found in [16]. (color online)

(OMC). Similarly, a set of lines found to be linear combinations of 22.7 Hz and 25.6 Hz in the L1 data was tracked down to digitization error in an OMC excitation at a still higher frequency.

Although most of these strong and narrow lines are stationary in frequency and hence do not exhibit the Doppler modulations due to the Earth's motion expected for a CW signal from most sky locations, they do degrade the sensitivity to astrophysical signals at the frequencies where they occur.

III. SIGNAL WAVEFORM

In this paper we assume a standard model of a spinning non-axisymmetric neutron star. Such a neutron star radiates circularly-polarized gravitational radiation along the rotation axis and linearly-polarized radiation in the directions perpendicular to the rotation axis. For the purposes of detection and establishing upper limits the linear polarization is the worst case, as such signals contribute the smallest amount of power to the detector.

The strain signal measured by a detector is

$$h(t) = h_0 \left(F_+(t,\alpha_0,\delta_0,\psi)\tfrac{1+\cos^2(\iota)}{2}\cos(\Phi(t)) + \right. \\ \left. + F_\times(t,\alpha_0,\delta_0,\psi)\cos(\iota)\sin(\Phi(t)) \right) , \quad (1)$$

where F_+ and $F_\times$ are the detector responses to signals with "+" and "×" quadrupolar polarizations [17–19], the sky location of the source is described by right ascension α_0 and declination δ_0, the inclination of the source rotation axis to the line of sight is ι, and we use ψ to denote the polarization angle (i.e. the projected source rotation axis in the sky plane).

The phase evolution of the signal is given by

$$\Phi(t) = 2\pi \left(f_0 \cdot (t-t_0) + f_0^{(1)} \cdot (t-t_0)^2/2 \right) + \phi \ , \quad (2)$$

with f_0 being the source frequency and $f_0^{(1)}$ denoting the first frequency derivative (which, when negative, is termed the *spindown*). We use t to denote the time in the Solar System barycenter frame. The initial phase ϕ is computed relative to reference time t_0. When expressed as a function of local time of ground-based

detectors, Equation 2 acquires sky-position-dependent Doppler shift terms.

Most natural "isolated" sources are expected to have negative first frequency derivative, due to the energy lost to emission of gravitational or electromagnetic radiation. The frequency derivative can be positive because of residual motions due to, for instance, a long-period orbit.

IV. THE MEDIUM SCALE LOOSELY COHERENT SEARCH

The medium scale loosely coherent search is the basic building-block of this search. It is described in [13] and follows earlier loosely coherent implementations [11, 12]. Here we highlight features that are useful to understand search output, in particular upper limits and outliers.

The input to the search are Hann-windowed 3600 s short Fourier transforms (SFTs) for each of the LIGO interferometers : $\{a_{tfi}\}$, indexed by time t, discrete frequencies f and interferometer index i. A value of the weighted power sum $P(f_0, \vec{p})$ is computed for every searched wave shape, parametrized by the frequency of the source f_0 and a set of values for its spindown, sky position and source orientation $\vec{p} = (\alpha, \delta, f_0^{(1)}, \iota)$.

The loosely coherent weighted power sum is a bilinear function of the SFT data:

$$P(f_0, \vec{p}) = \frac{\sum_{t_1,t_2,i_1,i_2} K(t_1, t_2, \vec{p}, f_0) a_{t_1 f_1' i_1} \bar{a}_{t_2 f_2' i_2}}{\sum_{t_1,t_2} W(t_1, t_2, \vec{p})}. \quad (3)$$

Here f_1' and f_2' are the interferometer-frame signal frequencies at the detector-time t_1 and t_2. The kernel $K(t_1, t_2, \vec{p}, f_0)$ is equivalent to a narrow band filter on the input data that includes phase corrections to account for the signals' Doppler shifts and relativistic effects. The weight term $W(t_1, t_2, \vec{p})$ folds-in the noise level of the individual SFTs and the detectors' response to the specific source as a function of time (it is fourth order in the antenna response). The explicit expressions for these functions are very involved not very illuminating without extensive additional information. We hence do not report them here but rather refer the interested reader to sections II - IV of [13].

Because the polarization coefficients are factored out of power sums (Eq. 3), which involve thousands of SFTs, it is easy to produce separate power sums for any polarization of interest. For instance, we will provide upper limits for a population of circularly polarized signals which corresponds to the star's rotation axis pointing towards us ($\iota = 0$ or π in Eq. 1).

The fact that we compute power sums makes it possible to set upper limits on the signal strain amplitude by estimating the power excess that we would measure from the target signals at a given strain amplitude. This estimate is computed using the universal statistics algorithm which produces statistically valid results without assumptions on the probability distribution function of the noise – a rigorous derivation of the algorithm is given in [20]. An intuitive explanation of why this is possible is that if the expected power of the noise is bounded, then the expectation of any continuous function of the noise is also bounded over the space of all probability distributions (in mathematical terminology the space of probability distributions is compact in weak topology). If the noise is Gaussian, the implementation of the *Universal* statistic used in this search provides close-to-optimal values.

In order to bracket the range of upper limit strain values, depending on the orientation of the source, we consider the so called "worst-" and "best-" case polarization upper limits. The upper limits are given as a function of frequency and apply to 0.125 Hz signal-frequency intervals, i.e. there is a single upper limit number for every 0.125 Hz band. The "worst-case" upper limits are based on the maximum universal statistic value over the frequencies in any given band and all spindowns, sky positions and polarizations, further increased (by 7%) to account for losses due to signal-template mismatch[1]. This maximization tends to select increased universal statistic values due to disturbances in the data, when present. For this reason the worst-case upper limit curve has larger outliers than the circular polarization ("best-case" one). The "best-case" upper limits are based on the maximum universal statistic value over the frequencies in any given the band and all spindowns and sky positions, while circular polarization is assumed.

The computation of universal statistic [20] also computes SNR as a byproduct, this is used as a detection statistic for identifying outliers.

V. SEARCH PIPELINE

We search a disk on the sky of radius 0.06 rad (3.43°) centered on right ascension 4.65 rad (266.42°) and declination −0.46 rad (−26.35°). This search area is chosen to cover both the globular cluster Terzan 5 and Sagittarius A*, galactic regions expected to contain many neutron stars. Terzan 5, in particular, has many known radio pulsars [21–23].

[1] The 7% is derived from the results of Monte Carlo simulations of this search on simulated signals[13].

Stage	Coherence length (hours)	Minimum SNR
0	8	6
1	12	6.5
2	16	7
3	24	8
4	36	9
5	48	11
6	72	13

TABLE I. Search pipeline
Parameters of search pipeline. As explained in the text stage 6 also features an additional consistency check between the single-detector statistics.

The search pipeline iteratively uses the medium scale loosely coherent algorithm in a cascade of 7 different stages. The first stage employs an 8 hour coherence length. Outliers identified at this stage are followed-up with more sensitive searches that utilise increasingly longer coherence lengths, as detailed in Table I. For all stages the detection statistic combines coherently over the coherent length the data from both detectors. At the last stage, the detection statistic from each detector separately is also computed and the additional requirement is set on surviving candidates that the parameters be consistent across the multi-detector and single-detector statistics. The consistency condition demands that outliers from the same sky point and spindown are no further than 5 μHz in frequency.

The pipeline is validated using extensive Monte Carlos that simulate signals in the real data and test the recovery efficiency of the whole pipeline. This approach is completely standard for this type of search, where the expected signals are weak and in many frequency bands it is impossible to model the noise reliably. This procedure also validates the correctness of the upper limit values given here.

A. Outlier ranking

The likelihood of a search outlier to have astrophysical origin is commonly described by the false alarm rate - an estimate of probability that this outlier is produced by pure chance. The most obvious method of computing this rate is to repeat the search many times with different realizations of the noise and count how many similar outliers are produced. This is impractical for broad parameter searches which usually take weeks to months to complete.

A commonly used shortcut is to reuse the data from the original search but combine it differently, for instance with non-astrophysical offsets for coincidence parameters (such as time or frequency) – for a notable example see [24]. The idea is to simulate different noise realisations of the search results, by constructing "off-source" combinations of the actual search results. Unfortunately, producing an "off-source" noise realization by combining the single-detector outliers from the last stage of this pipeline is not viable because the preceding stages are based on multi-detector statistics. This means that the outliers at the last stage present correlations between the frequencies of peaks in single-detector data. We want the artificially generated noise realisations (the off-source data) to also display such correlations. Unfortunately the standard methods to construct the off-source data by recombining the single-detector candidates with non-physical offsets would destroy such correlations, hence they are not suitable.

We take here a different approach and derive an approximate analytical expression, under the assumption that underlying noise is Gaussian. This is a strong assumption that is known not to hold in many frequency bands. Thus this expression should not be used as criterion for detection. Rather it is meant as a figure of merit to evaluate relative significance of outliers.

As the entire hierarchical 7-stage pipeline is difficult to model, we derive the false alarm rate for a hypothetical search that used the last stage of followup to analyze the entire parameter space. In the next paragraphs we describe the quantities that are necessary in order to estimate the false alarm rate Eq. 4. These quantities are: the total number of templates N that would have been used by the stage 6 search over the entire searched parameter space; the distribution of the detection statistic for the stage 6 search, $P_{\chi^2,k}$; the "coincidence probability" associated with the multi-detector/single-detector consistency check, $p_{\rm coinc}$. We derive these below.

We (over)-estimate the total number of templates N necessary to perform such search to be 1.6×10^{27}. We arrive at this number as follows: The total number of templates in the grid for the entire search over 1025 Hz, the whole sky, polarization and spindown is 9.3×10^{21}. We however search more waveforms than these because we additionally allow the frequency to change by up to one frequency bin 11 times, equally spaced throughout the observation period. This adds robustness to our search with respect to deviations of the real signal from a strictly coherent signal model. To account for this, we increase 9.3×10^{21} by a factor of 3^{11}. This overcounts the number of independent templates. For example, two templates different only by a single jump in frequency bin in the middle of the run, would be highly correlated.

Because we consider the last stage as a separate search the frequencies of outliers in individual interferometers are independent. The frequency coincidence criterion can be falsely triggered in pure noise with probability $p_{coinc} = 3.59\times10^{-5}$.

The last stage of the analysis uses a 3-day coherence time. As the variations in W (Eq. 3) due to amplitude modulations average out over this time, the power sums can be modelled as a χ^2 variable with at most $k = 80$ degrees of freedom, with k expected to be smaller for frequency regions with highly contaminated data. The reason for decrease in k is that the terms in the sum (Equation 3) containing contaminated data are de-weighted

and hence they contribute less than others to the total number of degrees of freedom. In the case of equal weighted data $k = 80$ because there are 40 3-day chunks in a 4-month run and each chunk contributes two degrees of freedom.

We take the Gaussian false alarm figure of merit for a candidate at signal-to-noise ratio value SNR, at the end of the last follow-up stage, to be

$$\begin{aligned}\log_{10}(\mathrm{GFA}) = \log_{10}\left(P_{\chi^2,k}\left(k+\sqrt{2k}\cdot\mathrm{SNR}\right)\right) + \\ +\log_{10}(N)+\log_{10}(p_{\mathrm{coinc}}),\end{aligned} \tag{4}$$

where SNR is defined as the ratio of the deviation of the detection statistic from its expected value to the standard deviation.

We emphasize again that the formula 4 was derived under the assumption of stationary Gaussian noise that is independent between the H1 and L1 interferometers. Since this assumption is violated in many frequency bands, this figure is not meant as a criteria for detection. For example, large negative values for outliers 1 through 8 are an indication of a presence of a signal, but these signals is known to be instrumental in origin.

VI. RESULTS

The search produces a number of outliers, the strongest of which are traced to clear instrumental artifacts. A number of unclassified outliers with smaller signal-to-noise ratios passes the follow-up pipeline. While the pipeline has been demonstrated to recover injected signals successfully even in the most heavily contaminated regions [13], the presence of noise does increase the false alarm rate. As the O1 data is highly contaminated with both stationary and non-stationary instrumental lines, classification of weak outliers is particularly difficult. This problem is made more challenging by the presence of instrumental artifacts coherent between both interferometers.

We further extend the coherent baseline of the search with ad-hoc semi-coherent follow-up searches like the ones used in [2, 3], on 352 outliers. We use three stages with coherent baselines of 210 hrs (12 segments), 500 hrs (6 segments) and 1260 hrs (2 segments), respectively. We denote the stages by FU0, FU1 and FU2. Since FU1 is rather computationally intensive we do not follow-up any outlier that can be associated with a disturbance (see comment field in the tables of Appendix A. 21 outliers survive all thresholds from these follow-up searches. The outlier with id 68 appears to be the most significant. On it we perform a dedicated search using the FU1 search on 480 hrs of the newly released data from the O2 run [8]. The search could not recover the candidate with detection statistic values consistent with what would have been expected if outlier 68 had been a continuous wave described by Eq. 1. Appendix A details all the outliers and indicates at what stage of these follow-ups the candidate was rejected.

The simulations described in [13] have shown that an astrophysical source adhering to expected signal model will be recovered within $15\,\mu$Hz of true frequency and within 1.5×10^{-11} Hz/s of true spindown. The sky position mismatch depends on frequency and, for outliers with frequency f is no more than $6.5\times10^{-4}\cdot(1\,\mathrm{kHz}/f)$ in ecliptic distance, defined as the distance between outlier location and true injection location after projection onto the ecliptic plane.

The universal statistic algorithm allows to set valid upper limits even in the most heavily contaminated bands. Figure 1 shows the best-case and worst-case 95% confidence upper limits on the signal strain in 0.125 Hz frequency intervals. At the highest frequency (1500 Hz) the worst-case upper limit on gravitational wave strain is 6.2×10^{-25}, which translates in a source with an ellipticity of 2.5×10^{-6} at 8.5 kpc. Because of maximization procedure the confidence level of the worst-case upper limits remains 95% or higher for any subset of parameters. For example, if one picks a sky location of the Terzan 5 globular cluster, spin-down of 5×10^{-9} Hz/s and a frequency of 550 Hz the worst case upper limit is 2.89×10^{-25} Hz , with a confidence level which is guaranteed to be at least 95%. The actual confidence level is likely to be larger than 95% for the specific point, because the quoted upper limit is the highest over all sampled spin-downs and the wider sky area.

Figure 2 shows the astrophysical reach of the search, i.e. the maximum distance at which this search could have detected a signal of a given frequency and spindown, under the assumption that all the lost rotational energy is emitted in gravitational waves. The search presented here is sensitive to an optimally oriented neutron star at the galactic center (circularly polarized signal) with ellipticity of 10^{-6} and emitting gravitational waves at a frequency of 1200 Hz. In Terzan 5 a signal at 1200 Hz from an optimally oriented source having ellipticity of $\leq 7\times10^{-7}$ could have been detected.

The search presented is the most sensitive to date, aimed at this interesting region of our galaxy. This is reflected in the sensitivity depth of the search which is defined as the ratio of the upper limit value and the noise floor at nearby frequencies $\mathcal{D}(f) := \sqrt{\frac{S_h(f)}{h_0^{UL}}}$ [25]. Following [26], we estimate the noise taking the harmonic mean across the different detectors and obtain the following values of the sensitivity depth across the entire frequency range searched:

$$\begin{cases}\mathcal{D}_{\texttt{circ-pol}}(f) & = 116\ \ [\sqrt{\mathrm{Hz}}]^{-1/2} \\ \mathcal{D}_{\texttt{worst-pol}}(f) & = 42\ \ [\sqrt{\mathrm{Hz}}]^{-1/2}.\end{cases} \tag{5}$$

The radiometer search [27] targeting the galactic center is 4 times less sensitive than our most conservative upper limit (the worst case one), achieving, on the same data, a sensitivity depth smaller than 10. This search covers a larger spindown range than any previously published all-sky search, hence probing younger sources from our search area. Furthermore even our worst-case upper lim-

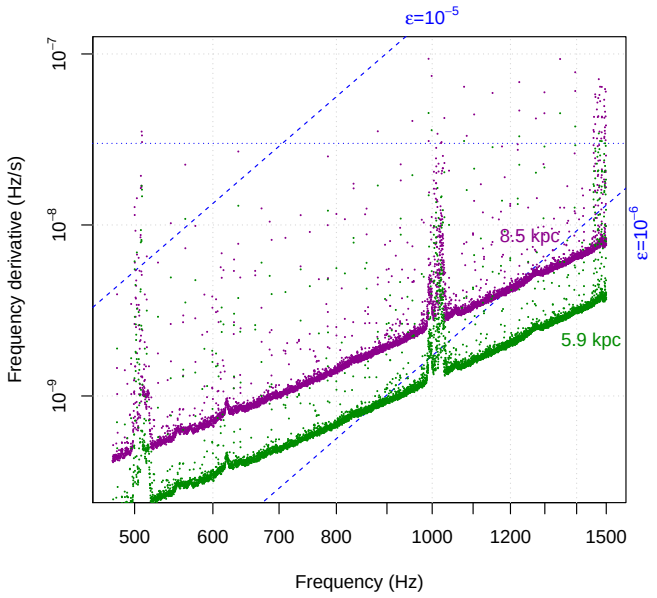

FIG. 2. Range of the search for neutron stars spinning down solely due to gravitational radiation. This is a superposition of two contour plots. The green (bottom) and purple (top) solid markers are contours of the maximum distance at which a neutron star could be detected as a function of gravitational-wave frequency f and its derivative $\dot{f}$. The dashed lines are contours of the corresponding ellipticity $\epsilon(f, \dot{f})$. The fine dotted line marks the maximum spindown searched. Together these quantities tell us the maximum range of the search in terms of various populations (see text for details) (color online). 5.9 kpc is the distance associated to many ATNF catalogue pulsars in the direction of Terzan 5.

its are more constraining than any all-sky search result to date, including the state of the art paper [28] that uses the more sensitive and longer duration data set from the O2 run.

VII. ACKNOWLEDGMENTS

The simulations and data analysis were performed on Atlas cluster at AEI Hannover, for which we thank Bruce Allen. We thank Carsten Aulbert and Henning Fehrmann for their support.

We thank Teviet Creighton and Keith Riles for many helpful comments and encouragement over the years.

The authors thank the LIGO Scientific Collaboration for access to the data and gratefully acknowledge the support of the United States National Science Foundation (NSF) for the construction and operation of the LIGO Laboratory and Advanced LIGO as well as the Science and Technology Facilities Council (STFC) of the United Kingdom, and the Max-Planck-Society (MPS) for support of the construction of Advanced LIGO. Additional support for Advanced LIGO was provided by the Australian Research Council.

This research has made use of data, software and/or web tools obtained from the LIGO Open Science Center (`https://losc.ligo.org`), a service of LIGO Laboratory, the LIGO Scientific Collaboration and the Virgo Collaboration. LIGO is funded by the U.S. National Science Foundation. Virgo is funded by the French Centre National de Recherche Scientifique (CNRS), the Italian Istituto Nazionale della Fisica Nucleare (INFN) and the Dutch Nikhef, with contributions by Polish and Hungarian institutes.

Appendix A: Outlier tables

Outliers passing all stages of automated followup from 475-1500 Hz band are separated into five tables. Table VI shows outliers inside the contaminated regions 495-520 Hz and 990-1033 Hz. The rest of the outliers is split into four regions 475-900 Hz, 900-1200 Hz, 1200-1400 Hz and 1400-1500 Hz (Tables II, III, IV, V).

Idx	SNR	$\log_{10}$(GFA)	Frequency Hz	Spindown nHz/s	RA_{J2000} degrees	DEC_{J2000} degrees	Description
6	23.9	-17.5	612.48610	−9.197	267.037	−29.754	Broad large line in L1 at 612.45 Hz
8	23.5	-16.6	736.09475	−22.991	267.808	−28.287	Sharp bin-centered lines at 736 Hz (H1) and 736.1 (L1)
13	21.2	-11.7	736.09791	−21.997	266.439	−29.165	Sharp bin-centered lines at 736 Hz (H1) and 736.1 (L1)
17	20.3	-9.6	684.96515	−17.607	265.576	−22.464	Sharp bin-centered line in L1 at 684.9 Hz
20	19.2	-7.5	662.18356	−24.621	263.548	−25.681	Strong bin-centered line in L1 at 662.20 Hz
24	17.9	-4.8	710.54465	−21.826	264.817	−27.547	Strong bin-centered line in L1 at 710.50 Hz
32	17.6	-4.0	599.19367	−15.234	266.039	−28.665	Large broad lines in H1 near 599.14 Hz and 599.16 Hz
34	17.5	-3.8	761.75580	−13.218	265.953	−25.889	Strong bin-centered line in L1 at 761.70 Hz (FU0)
43	16.8	-2.4	707.65162	−10.129	266.799	−24.227	Strong bin-centered line in L1 at 707.6 Hz
44	16.6	-2.1	575.23174	−5.519	266.534	−29.341	Hardware injected pulsar 2
45	16.6	-2.0	898.86970	−0.491	269.397	−28.914	Large broad lines in H1
47	16.5	-1.9	898.84667	−15.157	266.790	−26.909	Large broad lines in H1
70	15.2	0.8	659.35418	−12.386	269.229	−26.124	Strong bin-centered line in L1 at 659.3 Hz
72	15.1	0.9	629.86431	−29.241	267.817	−25.916	Large broad lines in L1
75	15.0	1.1	787.35687	−8.004	265.084	−29.806	Sharp bin-centered line in L1 at 787.3 Hz
80	14.8	1.4	660.51361	−20.472	268.538	−22.492	
84	14.8	1.5	829.85946	−8.609	264.856	−25.815	Strong bin-centered line in L1 at 829.8 Hz
85	14.8	1.5	520.84815	−3.204	267.198	−29.179	Large broad line in H1 near 520.82 Hz
89	14.7	1.7	520.84814	−3.201	267.202	−29.359	Large broad line in H1 near 520.82 Hz
99	14.5	2.1	763.94306	−20.331	262.960	−26.415	Hardware injected pulsar 9
102	14.5	2.1	873.26713	−29.286	264.627	−28.210	(FU0)
103	14.5	2.1	606.63606	−27.504	263.085	−27.581	Large broad line in H1 at 606.67 Hz
104	14.4	2.3	730.35349	−8.153	266.654	−26.898	Sharp bin-centered line in L1 at 730.3 Hz
119	14.2	2.7	787.35542	−8.931	264.431	−28.451	Sharp bin-centered line in L1 at 787.3 Hz
120	14.1	2.8	608.06595	−19.469	268.412	−28.434	Sharp bin-centered line in H1 at 608 Hz
121	14.1	2.8	899.25624	−27.714	263.423	−28.511	Strong broad lines in H1
135	14.0	3.1	599.49600	−17.127	267.287	−28.898	Strong broad lines in H1
137	14.0	3.1	771.05117	−8.789	265.082	−22.538	(FU1)
139	13.9	3.1	587.37228	−0.374	265.864	−29.281	(FU1)
145	13.9	3.2	864.06026	−9.286	262.769	−25.668	Sharp bin-centered line in H1 at 864 Hz
146	13.9	3.3	575.23399	−5.628	268.609	−27.074	Hardware injected pulsar 2
149	13.9	3.3	764.65686	−8.411	267.769	−27.209	Sharp bin-centered line in L1 at 764.6 Hz
151	13.9	3.3	817.31637	−23.376	267.491	−28.124	(FU1)
156	13.8	3.4	773.67502	−4.093	265.308	−23.202	
161	13.8	3.5	618.06167	−13.849	268.606	−25.285	Slope in H1 spectrum
166	13.8	3.5	738.02255	−0.388	263.204	−27.112	(FU0)
169	13.7	3.6	629.86433	−29.236	267.845	−26.116	Large broad line in L1
170	13.7	3.6	769.35342	−26.944	267.449	−22.402	(FU1)
172	13.7	3.6	686.75565	−11.731	264.065	−29.473	(FU0)
176	13.7	3.7	764.65687	−8.411	267.773	−27.188	Sharp bin-centered line in L1 at 764.6 Hz
180	13.6	3.7	683.40267	−12.421	265.532	−28.007	Slight slope in L1 (FU0)
186	13.6	3.8	799.26703	−5.724	266.255	−28.143	(FU0)
190	13.6	3.8	824.59028	−2.196	268.212	−27.435	(FU0)
192	13.6	3.8	645.94631	−15.366	266.741	−26.423	
202	13.5	3.9	727.32568	−17.438	267.008	−27.029	(FU1)
203	13.5	3.9	539.85863	−8.429	267.373	−29.396	Near 60 Hz line
215	13.5	4.1	851.68971	−18.266	266.383	−22.291	(FU1)
219	13.4	4.1	489.11959	−5.482	265.242	−25.347	Nearby lines
227	13.4	4.2	694.42637	−26.409	267.828	−27.898	(FU0)
229	13.4	4.2	581.71075	−9.491	263.276	−28.388	(FU1)
232	13.4	4.3	713.46388	−2.209	266.696	−26.761	Strong bin-centered line in L1 at 713.4 Hz
243	13.3	4.3	575.25658	−18.581	265.147	−29.940	Hardware injected pulsar 2
244	13.3	4.3	583.35870	−8.394	269.473	−29.052	Strong broad line in H1 at 583.317 (FU0)
248	13.3	4.4	763.95114	−21.211	266.312	−24.681	Hardware injected pulsar 9
249	13.3	4.4	680.27362	−14.639	263.404	−25.497	(FU0)
251	13.3	4.4	608.00120	−16.846	263.648	−28.505	Sharp bin-centered line in H1 at 608 Hz
254	13.3	4.4	770.00605	−19.542	264.245	−27.578	(FU1)
260	13.3	4.4	772.83474	−27.344	267.338	−26.027	Sharp bin-centered line in L1 at 772.8 Hz
261	13.3	4.4	809.98476	−27.979	263.634	−25.694	Sharp bin-centered line in L1 at 810 Hz
264	13.3	4.4	694.42638	−26.413	267.818	−27.711	(FU0)
270	13.3	4.5	878.16583	−14.756	267.454	−26.247	Strong bin-centered line in L1 at 878.1 Hz
282	13.2	4.5	547.67510	−9.729	263.964	−27.205	(FU0)
287	13.2	4.6	829.86026	−8.384	265.709	−27.241	Strong bin-centered line in L1 at 829.8 Hz
290	13.2	4.6	792.70263	−16.328	266.224	−29.232	(FU0)
291	13.2	4.6	655.43480	−2.403	263.896	−25.645	(FU0)
297	13.2	4.6	848.06291	−16.696	264.046	−26.114	Strong bin-centered line in H1 at 848 Hz
299	13.2	4.6	725.52768	−5.731	263.854	−25.707	(FU0)
303	13.2	4.6	782.79214	−20.134	265.043	−26.320	(FU1)
309	13.1	4.7	599.20398	−18.747	269.644	−26.805	Big broad lines in H1 near 599.14 and 599.16 Hz
310	13.1	4.7	698.22224	−22.943	263.921	−25.129	(FU0)
311	13.1	4.7	763.95114	−21.208	266.313	−24.999	Hardware injected pulsar 9
313	13.1	4.7	527.12774	−7.311	266.075	−25.556	(FU0)
316	13.1	4.8	753.97528	0.849	266.035	−25.250	(FU0)
317	13.1	4.8	844.15841	−9.201	262.865	−24.558	(FU1)
319	13.1	4.8	799.63851	−3.359	265.959	−29.050	(FU1)
323	13.1	4.8	718.02858	−22.968	266.134	−27.019	(FU1)
325	13.1	4.8	527.64148	−23.659	268.915	−24.650	(FU0)
335	13.0	4.9	621.85099	−11.539	266.052	−27.996	Sloping H1 spectrum
337	13.0	4.9	676.37758	−0.769	268.788	−24.882	(FU0)
340	13.0	4.9	678.39254	−3.871	263.974	−28.642	

TABLE II. Outliers below 900 Hz that passed the automated detection pipeline excluding regions heavily contaminated with violin modes. Outliers marked with "line" had strong narrowband disturbances identified near the outlier location. We have marked outliers not consistent with the target signals at one of the semi-coherent $\mathcal{F}$-statistic follow-ups with "(FU0/1/2)", depending on the stage at which they did not pass the detection thresholds. Frequencies are converted to epoch GPS 1130529362.

Idx	SNR	$\log_{10}$(GFA)	Frequency Hz	Spindown nHz/s	RA_{J2000} degrees	DEC_{J2000} degrees	Description
5	25.2	-20.4	1176.69799	−26.024	264.288	−23.567	Strong bin-centered line in L1 at 1176.6 Hz
16	20.8	-10.8	955.00851	−26.744	269.405	−24.278	Sharp line in L1
19	19.3	-7.6	910.17153	−8.556	264.028	−24.077	Large broad line in H1 at 910.1 Hz
33	17.5	-4.0	1176.58614	−3.254	263.501	−25.977	Strong bin-centered line in L1 at 1176.6 Hz
39	17.0	-2.9	1120.09915	−25.758	264.594	−27.448	Strong bin-centered line in H1 at 1120 Hz
40	16.9	-2.6	910.18376	−22.563	268.269	−25.989	Large broad line in H1 at 910.1 Hz
58	15.5	0.1	1173.80211	−28.189	264.045	−27.467	Strong bin-centered line in L1 at 1173.7 Hz
59	15.5	0.1	1128.38343	−12.747	267.927	−27.526	Strong bin-centered line in L1 at 1128.3 Hz
63	15.3	0.4	906.63379	−17.648	264.077	−23.762	Strong bin-centered line in L1 at 906.6 Hz
68	15.2	0.6	1105.15733	−26.774	263.713	−26.330	(FU1 w. O2 data)
76	15.0	1.2	1128.39396	−25.644	263.670	−27.537	Strong bin-centered line in L1 1128.3 Hz
77	14.9	1.3	946.92321	−20.521	266.068	−27.668	(FU0)
81	14.8	1.4	977.67244	−18.241	264.215	−26.981	Strong bin-centered line in L1 at 977.6 Hz
86	14.7	1.6	1130.32268	−1.751	267.651	−29.016	(FU0)
101	14.5	2.1	983.46951	−11.611	264.204	−23.932	Strong bin-centered line in L1 at 983.4 Hz
106	14.4	2.3	976.01956	−26.851	265.826	−29.672	Line in H1 at 976 Hz
113	14.3	2.5	957.88553	−2.921	266.766	−24.376	Sharp bin-centered line in L1 at 957.8 Hz
114	14.3	2.5	932.28876	−0.777	265.303	−25.123	Sharp bin-centered line in L1 at 932.2 Hz
116	14.2	2.6	1083.85197	−19.421	266.328	−24.585	(FU0)
118	14.2	2.7	1117.93710	−29.371	266.174	−24.014	
125	14.1	2.9	1192.54799	0.039	267.676	−26.744	(FU0)
126	14.1	2.9	1144.81799	−12.261	265.508	−28.590	(FU0)
130	14.0	3.0	1146.01080	−14.459	264.505	−26.227	(FU1)
133	14.0	3.1	1056.49144	−6.807	263.080	−25.072	(FU1)
143	13.9	3.2	916.79125	−21.067	266.033	−24.889	(FU0)
147	13.9	3.3	1055.06400	−21.219	267.870	−25.985	(FU0)
148	13.9	3.3	1148.12864	−9.921	268.460	−28.864	Strong bin-centered line in L1 at 1148.1 Hz
158	13.8	3.4	1193.00546	−15.631	266.493	−25.264	(FU0)
159	13.8	3.5	911.76958	−9.399	266.039	−25.180	(FU0)
160	13.8	3.5	1130.73154	−3.169	263.000	−26.335	(FU0)
162	13.8	3.5	953.40039	−10.813	266.270	−27.596	
174	13.7	3.6	1087.75530	−28.077	269.614	−26.525	(FU2)
181	13.6	3.7	969.52238	−8.313	265.371	−29.459	(FU0)
206	13.5	4.0	1159.91542	−24.221	264.096	−25.279	(FU0)
208	13.5	4.0	1142.86654	−6.054	263.246	−24.169	(FU0)
210	13.5	4.0	934.78261	−2.273	268.362	−25.152	(FU0)
211	13.5	4.0	1080.01473	−27.759	266.170	−28.283	Strong coincident bin-centered lines in H1 and L1 at 1080 Hz
213	13.5	4.1	1127.80227	−19.557	267.194	−23.981	(FU1)
223	13.4	4.2	970.66243	−29.248	266.863	−25.559	(FU0)
228	13.4	4.2	931.29979	−10.836	266.227	−29.987	
233	13.4	4.3	1151.53614	−8.588	265.597	−23.441	
237	13.3	4.3	1145.63773	−5.498	268.460	−29.377	(FU0)
242	13.3	4.3	983.47659	−7.236	265.003	−27.225	Strong bin-centered line in L1 at 983.4 Hz
245	13.3	4.3	1197.77064	−27.963	269.015	−27.561	
253	13.3	4.4	903.29002	−15.369	266.450	−25.044	(FU0)
258	13.3	4.4	938.88434	−9.556	264.187	−28.599	(FU0)
265	13.3	4.4	953.40039	−10.816	266.269	−27.442	
266	13.3	4.5	906.90104	−20.814	263.359	−26.506	Broad line in H1 near 906.82 Hz
267	13.3	4.5	1069.13874	−2.926	263.432	−27.102	
272	13.2	4.5	1033.96710	−20.787	262.779	−25.972	(FU0)
273	13.2	4.5	1039.41470	0.882	267.926	−24.697	
276	13.2	4.5	1121.71865	−15.156	263.124	−27.755	(FU0)
279	13.2	4.5	1102.25911	−26.261	266.982	−27.473	(FU1)
284	13.2	4.5	1055.96111	−20.166	266.229	−28.653	(FU0)
285	13.2	4.5	1081.91076	−29.388	264.805	−29.647	(FU0)
295	13.2	4.6	1143.15676	−5.409	269.119	−26.704	(FU1)
300	13.2	4.6	951.01213	−4.077	266.334	−28.538	(FU0)
305	13.2	4.7	1070.50637	−4.409	264.544	−27.297	
307	13.1	4.7	1123.01894	−10.841	268.163	−24.666	(FU0)
314	13.1	4.7	945.03386	−24.222	267.786	−26.393	Bump in L1
318	13.1	4.8	989.77830	−4.182	269.861	−25.516	Disturbed H1 spectrum
330	13.1	4.8	1176.33662	−22.274	264.698	−27.271	(FU1)
336	13.0	4.9	985.14327	−23.229	265.622	−26.558	Many strong nearby lines in H1
338	13.0	4.9	1090.81873	−0.502	264.444	−29.353	(FU0)
339	13.0	4.9	1196.00279	−2.451	267.251	−24.656	(FU0)
342	13.0	4.9	1037.60585	−26.743	263.801	−28.995	Strong bin-centered line in L1 at 1037.5 Hz
350	13.0	4.9	1197.48407	−23.759	269.911	−25.523	

TABLE III. Outliers in frequency range 900-1200 Hz that passed the detection pipeline excluding regions heavily contaminated with violin modes. Outliers marked with "line" had strong narrowband disturbances identified near the outlier location. We have marked outliers not consistent with the target signals at one of the semi-coherent $\mathcal{F}$-statistic follow-ups with "(FU0/1/2)", depending on the stage at which they did not pass the detection thresholds. Frequencies are converted to epoch GPS 1130529362.

Idx	SNR	$\log_{10}$(GFA)	Frequency Hz	Spindown nHz/s	RA_{J2000} degrees	DEC_{J2000} degrees	Description
1	30.5	-32.4	1220.62344	−16.068	265.994	−24.436	Induced by hardware injection 7 (FU0)
37	17.0	-2.9	1360.09284	−16.252	262.922	−27.103	Strong bin-centered line in H1 at 1360 Hz
42	16.8	-2.5	1276.22672	−0.304	268.176	−23.187	Strong bin-centered line in L1 at 1276.1 Hz
55	15.8	-0.4	1202.29927	−6.043	264.510	−24.894	Strong bin-centered line in L1 at 1202.2 Hz
56	15.7	-0.2	1376.12253	−4.253	269.645	−26.036	Strong bin-centered line in H1 at 1376 Hz
67	15.3	0.6	1280.12932	0.519	268.744	−23.550	Strong bin-centered line in H1 at 1280 Hz
69	15.2	0.8	1270.39556	−12.976	268.516	−24.920	Strong bin-centered line in L1 at 1270.3 Hz
78	14.9	1.3	1328.13275	0.159	269.294	−26.578	Strong bin-centered line in H1 at 1328 Hz
82	14.8	1.5	1202.29985	−5.886	264.920	−25.698	Strong bin-centered line in L1 at 1202.2 Hz
91	14.7	1.8	1376.09811	−20.913	267.292	−26.665	Strong bin-centered line in H1 at 1376 Hz (FU0)
93	14.6	1.8	1355.19792	−22.717	265.274	−27.347	(FU1)
96	14.6	2.0	1303.93001	−13.662	268.017	−29.082	(FU0)
107	14.3	2.4	1321.58965	−19.634	263.445	−25.948	Strong bin-centered line in L1 at 1321.5 Hz
111	14.3	2.5	1352.11873	−4.071	266.570	−28.811	Bin-centered line in H1 at 1352 Hz
112	14.3	2.5	1254.44064	−15.222	265.991	−25.692	(FU1)
115	14.2	2.6	1301.62221	−15.454	265.848	−28.031	
117	14.2	2.6	1202.30356	−26.059	267.238	−23.480	Strong bin-centered line in L1 at 1202.2 Hz
123	14.1	2.9	1270.39317	−17.622	268.335	−25.117	Strong bin-centered line in L1 at 1270.3 Hz
127	14.0	3.0	1386.49465	−13.231	267.856	−23.177	(FU0)
128	14.0	3.0	1380.26131	−19.417	263.195	−24.722	(FU0)
129	14.0	3.0	1264.07644	−19.604	265.130	−29.366	Line in at 1264 Hz in H1
138	13.9	3.1	1249.43252	−2.559	265.309	−23.949	(FU0)
140	13.9	3.2	1373.86300	−7.084	263.597	−27.357	(FU0)
141	13.9	3.2	1205.72493	−26.927	264.610	−28.241	(FU0)
142	13.9	3.2	1271.07364	−17.608	266.148	−28.676	(FU0)
144	13.9	3.2	1366.55954	−0.596	262.870	−26.589	(FU0)
150	13.9	3.3	1331.30890	−21.827	263.364	−28.484	(FU1)
152	13.8	3.4	1264.10309	−6.094	262.596	−26.501	Strong bin-centered line in H1 at 1264 Hz
163	13.8	3.5	1315.28928	−21.894	270.072	−25.232	(FU0)
165	13.8	3.5	1380.26131	−19.417	263.200	−24.633	(FU0)
171	13.7	3.6	1269.91895	−21.536	267.428	−28.206	(FU0)
173	13.7	3.6	1276.99016	−0.241	265.645	−29.501	(FU1)
175	13.7	3.7	1332.83814	−16.049	265.781	−27.931	(FU0)
177	13.7	3.7	1372.18144	−19.329	264.461	−27.028	(FU1)
179	13.7	3.7	1267.04168	−8.514	268.806	−23.928	(FU0)
182	13.6	3.7	1232.09595	−8.929	266.351	−26.068	Strong bin-centered line in H1 at 1232 Hz
188	13.6	3.8	1254.44064	−15.229	265.990	−25.311	(FU1)
189	13.6	3.8	1394.57034	−8.916	269.267	−23.752	(FU1)
191	13.6	3.8	1270.38626	−19.122	263.603	−25.026	Strong bin-centered line in L1 at 1270.3 Hz
194	13.6	3.8	1318.61537	−2.694	263.896	−27.405	Line in L1 at 1318.6 Hz ???
195	13.6	3.9	1262.65832	−14.294	266.151	−27.129	(FU0)
199	13.5	3.9	1212.89760	−9.841	262.769	−25.319	(FU1)
207	13.5	4.0	1202.29841	−27.188	263.136	−26.481	Strong bin-centered line in L1 at 1202.2 Hz
214	13.5	4.1	1232.09153	−18.288	268.914	−24.416	Strong bin-centered line in H1 at 1232 Hz
218	13.5	4.1	1270.38624	−19.118	263.585	−25.347	Strong bin-centered line in L1 at 1270.3 Hz
220	13.4	4.1	1313.36532	0.507	266.019	−23.381	(FU0)
236	13.3	4.3	1242.80188	0.099	263.747	−28.690	(FU0)
238	13.3	4.3	1210.06445	−0.084	264.836	−26.046	
241	13.3	4.3	1317.50608	−14.391	267.541	−28.868	(FU0)
246	13.3	4.3	1280.91794	−20.272	265.138	−29.732	(FU1)
247	13.3	4.4	1222.09162	−9.369	268.642	−26.238	Strong bin-centered line in L1 at 1222 Hz
255	13.3	4.4	1253.01107	−5.959	265.096	−25.776	
257	13.3	4.4	1323.77888	0.764	268.106	−29.354	(FU0)
262	13.3	4.4	1253.01107	−5.964	265.098	−25.512	(FU0)
263	13.3	4.4	1261.98690	−6.648	265.929	−24.334	(FU0)
269	13.3	4.5	1329.92157	−2.304	264.893	−25.113	(FU0)
271	13.2	4.5	1371.33276	−6.367	267.733	−27.949	(FU0)
274	13.2	4.5	1299.81900	−3.076	265.372	−26.913	(FU0)
278	13.2	4.5	1289.14048	−18.428	265.039	−27.429	(FU0)
283	13.2	4.5	1292.03374	−18.191	263.987	−24.625	(FU0)
286	13.2	4.6	1298.51021	−3.954	269.268	−26.330	(FU0)
288	13.2	4.6	1321.82947	−26.962	267.202	−26.389	
289	13.2	4.6	1399.83041	−29.214	264.793	−29.091	
293	13.2	4.6	1247.68962	−21.128	265.493	−23.383	Strong bin-centered line in L1 at 1247.6 Hz (FU0)
294	13.2	4.6	1225.38754	−28.327	264.042	−25.595	(FU0)
298	13.2	4.6	1359.45910	−2.732	266.847	−26.802	(FU0)
308	13.1	4.7	1282.33163	−13.246	263.533	−26.441	(FU0)
322	13.1	4.8	1225.72267	−17.528	263.821	−25.398	(FU0)
327	13.1	4.8	1249.95109	−23.121	266.789	−27.051	(FU1)
331	13.1	4.8	1297.00050	−1.628	267.856	−26.736	(FU0)
332	13.1	4.8	1215.84097	−17.271	269.914	−27.022	(FU0)
333	13.0	4.9	1295.23973	−11.871	266.940	−28.091	(FU0)
334	13.0	4.9	1306.38413	−18.809	265.273	−22.916	(FU0)
341	13.0	4.9	1345.96737	−26.084	263.623	−26.514	(FU1)
343	13.0	4.9	1216.27144	−10.614	267.855	−25.711	(FU0)
344	13.0	4.9	1259.45564	−9.417	267.383	−28.047	(FU0)
345	13.0	4.9	1235.24532	−0.544	263.166	−27.175	(FU1)
347	13.0	4.9	1308.95261	−3.621	264.053	−25.778	(FU0)
348	13.0	4.9	1324.98925	−27.563	267.805	−28.168	(FU0)
349	13.0	4.9	1272.22405	−27.694	264.174	−27.709	
351	13.0	4.9	1334.41973	−22.024	262.929	−28.009	(FU0)

TABLE IV. Outliers in frequency range 1200-1400 Hz that passed the detection pipeline excluding regions heavily contaminated with violin modes. Outliers marked with "line" had strong narrowband disturbances identified near the outlier location. We have marked outliers not consistent with the target signals at one of the semi-coherent $\mathcal{F}$-statistic follow-ups with "(FU0/1/2)", depending on the stage at which they did not pass the detection thresholds. Frequencies are converted to epoch GPS 1130529362.

Idx	SNR	$\log_{10}$(GFA)	Frequency Hz	Spindown nHz/s	RA_{J2000} degrees	DEC_{J2000} degrees	Description
2	27.8	-26.2	1457.98771	−5.923	267.265	−23.236	Broad line in L1
3	27.5	-25.5	1495.87736	−19.359	263.979	−25.411	Broad line in L1
12	21.6	-12.6	1469.41404	−12.041	267.020	−24.399	Strong bin-centered line in L1 at 1469.3 Hz
15	20.9	-11.0	1467.55257	−19.926	265.951	−29.741	Broad disturbance in H1 (?)
18	20.2	-9.6	1469.44100	−1.796	269.546	−24.514	Strong bin-centered line in L1 at 1469.3 Hz
21	19.1	-7.1	1421.11633	−6.941	263.048	−26.468	Strong bin-centered line in L1 at 1421 Hz
23	18.1	-5.1	1478.75395	−0.269	268.825	−26.084	Broad line in H1
26	17.8	-4.4	1469.40683	−14.406	263.178	−26.341	Strong bin-centered line in L1 at 1469.3 Hz
29	17.7	-4.3	1421.11841	−6.437	264.313	−27.030	Strong bin-centered line in L1 at 1421 Hz
30	17.6	-4.2	1408.10431	−25.129	266.189	−23.920	Strong bin-centered line in H1 at 1408 Hz
35	17.4	-3.6	1418.20292	−20.386	267.609	−24.774	Strong bin-centered line in L1 at 1418.1 Hz
36	17.1	-3.1	1421.11841	−6.436	264.313	−27.043	Strong bin-centered line in L1 at 1421 Hz
41	16.8	-2.5	1484.50512	−6.777	269.295	−26.268	Broad line in H1
53	16.2	-1.2	1467.47364	−1.878	268.521	−27.384	Broad line in H1
60	15.5	0.2	1478.75226	−0.909	267.825	−27.981	Broad line in H1
62	15.4	0.3	1499.44086	−7.311	263.883	−25.493	Nearby broad lines in H1 and L1
73	15.0	1.1	1484.75642	−29.816	265.225	−26.457	Broad line in H1
74	15.0	1.1	1401.69854	−22.076	264.511	−26.586	(FU1)
88	14.7	1.7	1458.95808	−15.962	268.240	−26.171	
90	14.7	1.8	1400.73383	−8.001	268.040	−25.138	(FU1)
92	14.6	1.8	1492.34125	−8.216	266.388	−23.361	Broad line in L1
94	14.6	1.9	1497.84101	−4.821	263.660	−28.526	Broad line in L1
100	14.5	2.1	1484.48710	−0.763	267.286	−27.112	Broad lines in H1
132	14.0	3.1	1443.81841	−9.151	268.034	−25.533	Strong bin-centered line in L1 at 1443.7 Hz
136	14.0	3.1	1497.84102	−4.823	263.665	−28.451	Broad line in L1
154	13.8	3.4	1498.67420	−19.913	264.048	−23.412	Broad line in H1
167	13.7	3.5	1472.02303	−12.624	263.554	−25.278	Broad line in L1
183	13.6	3.7	1402.87061	−20.561	269.872	−26.485	
193	13.6	3.8	1457.63610	−4.906	263.216	−24.295	Broad line in L1
196	13.6	3.9	1454.89391	−20.218	268.541	−25.625	
198	13.5	3.9	1442.61715	−16.934	267.499	−25.456	
200	13.5	3.9	1462.09124	−28.426	264.860	−27.360	Broad line in H1
201	13.5	3.9	1488.98202	−9.992	265.988	−27.058	(FU0)
204	13.5	3.9	1443.50058	−8.113	268.399	−26.734	(FU0)
205	13.5	4.0	1496.13532	−8.503	264.346	−26.994	Broad line in L1
209	13.5	4.0	1499.43021	−15.954	264.590	−25.146	Nearby broad lines in H1 and L1
216	13.5	4.1	1498.67734	−21.961	267.824	−29.502	Broad line in H1
224	13.4	4.2	1499.42849	−16.246	263.688	−28.354	Nearby broad lines in H1 and L1
226	13.4	4.2	1489.97625	−29.213	269.022	−24.757	(FU0)
230	13.4	4.2	1465.36884	−1.351	266.338	−23.042	(FU0)
231	13.4	4.3	1408.12849	−2.961	264.812	−28.640	Strong bin-centered line in H1 at 1408 Hz
235	13.3	4.3	1482.00682	−4.574	263.839	−26.682	Disturbed spectrum in H1
239	13.3	4.3	1408.10786	−17.896	270.286	−26.385	Strong bin-centered line in H1 at 1408 Hz
250	13.3	4.4	1459.40166	−29.472	269.924	−27.156	(FU0)
252	13.3	4.4	1460.13953	−25.686	267.954	−26.966	(FU0)
256	13.3	4.4	1408.11002	−10.656	268.386	−27.919	Strong bin-centered line in H1 at 1408 Hz
259	13.3	4.4	1482.62319	−22.633	264.730	−27.878	Nearby broad line in H1
268	13.3	4.5	1445.84829	−16.384	268.512	−28.667	(FU0)
275	13.2	4.5	1474.29669	−28.242	265.215	−26.055	Nearby broad line in H1, disturbed H1 spectrum
277	13.2	4.5	1462.20888	−19.916	268.963	−25.106	(FU0)
296	13.2	4.6	1478.10769	−26.661	265.631	−22.822	Bin-centered line in L1 at 1478 Hz, disturbed H1 spectrum
301	13.2	4.6	1459.94553	−3.364	265.599	−29.328	(FU0)
302	13.2	4.6	1455.78804	−1.216	263.403	−28.173	(FU1)
312	13.1	4.7	1472.96626	−6.889	263.067	−25.410	(FU1)
320	13.1	4.8	1432.48786	−23.659	267.769	−28.544	(FU0)
321	13.1	4.8	1496.76907	−17.039	262.628	−26.112	(FU0)
324	13.1	4.8	1499.42798	−18.013	268.803	−25.498	Nearby broad lines in H1 and L1
326	13.1	4.8	1475.08910	−24.164	268.123	−29.057	Nearby strong line in H1, disturbed spectrum
328	13.1	4.8	1430.12480	−23.206	266.342	−24.490	
329	13.1	4.8	1430.12480	−23.204	266.342	−24.625	(FU0)
346	13.0	4.9	1423.41985	−2.116	264.904	−26.065	(FU0)
352	13.0	4.9	1499.10849	−0.374	267.745	−26.798	Broad line in L1

TABLE V. Outliers above 1400 Hz that passed the detection pipeline excluding regions heavily contaminated with violin modes. Outliers marked with "line" had strong narrowband disturbances identified near the outlier location. We have marked outliers not consistent with the target signals at one of the semi-coherent $\mathcal{F}$-statistic follow-ups with "(FU0/1/2)", depending on the stage at which they did not pass the detection thresholds. Frequencies are converted to epoch GPS 1130529362.

Idx	SNR	$\log_{10}$(GFA)	Frequency Hz	Spindown nHz/s	RA_{J2000} degrees	DEC_{J2000} degrees	
4	27.3	-25.0	508.26088	−9.104	269.109	−29.202	Broad line in H1 at 508.222
7	23.6	-16.9	1030.75807	−24.288	265.630	−28.137	Forest of strong lines in L1
9	23.2	-16.0	501.54872	−22.486	264.981	−23.309	Large line in H1, violin mode region
10	22.7	-14.9	1018.71452	−13.869	268.055	−23.245	Strong line in L1
11	22.0	-13.4	505.62039	−6.776	264.643	−27.775	Large lines in H1, violin mode region
14	21.0	-11.2	1027.44609	−28.797	266.018	−29.859	Forest of strong lines in L1
22	18.9	-6.7	1014.13265	−5.347	269.223	−28.565	Forest of strong lines in L1
25	17.9	-4.7	1030.76062	−27.591	269.921	−27.663	Forest of strong lines in L1
27	17.7	-4.4	505.63342	−0.324	266.622	−29.454	Large lines in H1, violin mode region
28	17.7	-4.3	505.68386	−20.164	267.657	−25.001	Large lines in H1, violin mode region
31	17.6	-4.1	1008.58625	0.313	263.517	−27.178	Strong broad line in H1, line in L1
38	17.0	-2.9	505.72151	−16.584	265.219	−27.670	Large line in H1, violin mode region
46	16.5	-1.9	1006.00395	−14.306	267.233	−27.920	Strong broad lines in H1
48	16.5	-1.9	1021.20375	−22.584	267.795	−24.931	Lines in L1
49	16.4	-1.7	509.19731	0.039	266.911	−29.803	Violin mode region
50	16.3	-1.5	1031.08895	−27.254	263.465	−24.793	Lines in L1
51	16.3	-1.5	506.97395	−12.404	265.161	−27.594	Large line in H1, violin mode region
52	16.3	-1.4	1027.53960	−15.576	269.243	−24.104	Forest of strong lines in L1
54	15.8	-0.6	509.19626	−0.289	264.906	−26.767	Violin mode region
57	15.6	-0.2	1017.17041	−15.632	263.374	−24.850	
61	15.4	0.3	1029.13774	−21.237	263.826	−28.459	Forest of strong lines in L1 (FU0)
64	15.3	0.5	505.72844	−13.179	267.146	−23.848	Large broad and narrow lines in H1, L1, violin mode region
65	15.3	0.5	1027.53447	−15.899	264.371	−27.442	Forest of strong lines in L1
66	15.3	0.6	1014.13550	−0.511	269.734	−28.397	Forest of strong lines in L1
71	15.1	0.9	992.02121	−22.994	269.830	−28.298	Strong broad line in H1, lines in L1
79	14.9	1.4	503.01053	−14.412	264.576	−29.521	Large lines in H1, violin mode region
83	14.8	1.5	1006.18012	−21.694	263.313	−24.036	Strong bin-centered line in L1 at 1006.1 Hz
87	14.7	1.6	1030.76044	−17.694	264.609	−25.125	Forest of strong lines in L1
95	14.6	1.9	1003.74867	−4.776	265.096	−24.430	Strong broad line in H1
97	14.6	2.0	1013.03947	−0.404	268.508	−28.026	Disturbed background in H1
98	14.5	2.0	1026.14462	−28.021	267.878	−27.584	Broad line in L1
105	14.4	2.3	1004.02592	−2.816	265.980	−25.168	(FU0)
108	14.3	2.4	1004.02591	−2.814	265.980	−25.265	(FU0)
109	14.3	2.4	1003.73614	−16.516	266.800	−28.487	Strong broad line in H1
110	14.3	2.5	1029.19672	1.012	270.018	−27.237	Forest of lines in L1
122	14.1	2.8	993.55783	−25.844	265.053	−24.977	(FU0)
124	14.1	2.9	511.99612	−0.903	266.165	−25.709	Sharp bin-centered line at 512 Hz
131	14.0	3.0	1000.06619	−13.539	266.692	−26.396	Lines in H1 and L1
134	14.0	3.1	1011.00509	−18.583	269.680	−25.059	Strong line in L1, disturbed H1 spectrum
153	13.8	3.4	1003.75296	−3.369	265.458	−27.670	Strong broad line in H1
155	13.8	3.4	1025.63609	−7.339	265.091	−23.025	Forest of lines in L1
157	13.8	3.4	994.50537	−0.149	264.616	−28.649	(FU0)
164	13.8	3.5	990.28898	−0.769	264.972	−26.915	Disturbed H1 spectrum
168	13.7	3.5	1031.39556	−7.501	263.845	−23.332	Forest of lines in L1
178	13.7	3.7	1010.61505	−17.337	265.335	−24.634	Disturbed H1 spectrum, lines in L1
184	13.6	3.8	991.26021	−23.166	266.511	−27.602	Disturbed H1 spectrum, lines
185	13.6	3.8	1006.00396	−14.314	267.225	−27.634	Strong broad lines in H1, lines in L1
187	13.6	3.8	1031.16138	−14.838	264.511	−23.556	Forest of lines in L1
197	13.6	3.9	509.19895	0.414	269.633	−27.167	Large lines, violin mode region
212	13.5	4.0	1017.38348	−16.619	268.845	−24.206	(FU0)
217	13.5	4.1	1018.82920	−17.391	264.399	−26.832	(FU0)
221	13.4	4.1	1011.02816	−16.411	267.760	−22.824	Disturbed H1 spectrum, lines in L1
222	13.4	4.1	1016.77536	−0.176	267.870	−23.024	(FU0)
225	13.4	4.2	993.08901	−25.739	269.788	−25.063	(FU1)
234	13.4	4.3	992.25622	−22.391	265.644	−27.798	Forest of lines in H1 and L1
240	13.3	4.3	1005.02179	−22.107	269.152	−28.822	(FU0)
280	13.2	4.5	1031.49141	−25.294	266.685	−27.054	Forest of lines in L1
281	13.2	4.5	1013.13666	−22.974	268.774	−25.644	Large disturbance in H1
292	13.2	4.6	997.43474	−5.569	266.898	−26.932	Strong bin-centered line in L1 at 997.4, disturbed H1 spectrum
304	13.2	4.6	1002.78826	−1.404	268.608	−27.280	Strong line in L1
306	13.1	4.7	1000.06213	−15.341	264.654	−27.047	Lines in H1 and L1 (FU0)
315	13.1	4.7	991.62069	−12.746	263.013	−27.125	Strong broad line in L1

TABLE VI. Outliers in 495-520 Hz and 990-1033 Hz regions heavily contaminated with violin modes. Outliers marked with "line" had strong narrowband disturbances identified near the outlier location. We have marked outliers not consistent with the target signals at one of the semi-coherent $\mathcal{F}$-statistic follow-ups with "(FU0/1/2)", depending on the stage at which they did not pass the detection thresholds. Frequencies are converted to epoch GPS 1130529362.

[1] Recent searches for continuous gravitational waves, K. Riles, Mod. Phys. Lett. A **32** 1730035 (2017).

[2] First low-frequency Einstein@Home all-sky search for continuous gravitational waves in Advanced LIGO data, B. P. Abbott *et al.* (LIGO Scientific Collaboration and Virgo Collaboration), Phys. Rev. D **96** 122004 (2017)

[3] All-sky search for periodic gravitational waves in the O1 LIGO data, B. P. Abbott *et al.* (LIGO Scientific Collaboration and Virgo Collaboration), Phys. Rev. D **96** 062002 (2017).

[4] Full Band All-sky Search for Periodic Gravitational Waves in the O1 LIGO Data, B. P. Abbott *et al.* (LIGO Scientific Collaboration and Virgo Collaboration), Phys. Rev. D **97** 102003 (2018).

[5] First loosely coherent all-sky search for periodic gravitational waves in the O1 LIGO data, V. Dergachev, M.A. Papa, `https://arxiv.org/abs/1902.05530`, submitted to PRL.

[6] A search of the Orion spur for continuous gravitational waves using a "loosely coherent" algorithm on data from LIGO interferometers J. Aasi *et al.* (LIGO Scientific Collaboration and Virgo Collaboration), Phys. Rev. D **93**, 042006 (2016).

[7] M. Vallisneri *et al.* "The LIGO Open Science Center", proceedings of the 10th LISA Symposium, University of Florida, Gainesville, May 18-23, 2014, arxiv:1410.4839.

[8] https://doi.org/10.7935/CA75-FM95LIGO Open Science Center, `https://losc.ligo.org`.

[9] Advanced LIGO, J. Aasi *et al.* (LIGO Scientific Collaboration), Class. Quantum Grav. **32** 7 (2015) .

[10] GW150914: The Advanced LIGO Detectors in the Era of First Discoveries, B. P. Abbott *et al.* (LIGO Scientific Collaboration and Virgo Collaboration), Phys. Rev. Lett. **116** 131103 (2016).

[11] On blind searches for noise dominated signals: a loosely coherent approach, V. Dergachev, Class. Quantum Grav. **27**, 205017 (2010).

[12] Loosely coherent searches for sets of well-modeled signals, V. Dergachev, Phys. Rev. D **85**, 062003 (2012).

[13] Efficient loosely coherent searches for medium scale coherence lengths, V. Dergachev, `https://arxiv.org/abs/1807.02351`, submitted to PRD.

[14] Maximum elastic deformations of relativistic stars, N.K. Johnson-McDaniel and B.J. Owen, Phys. Rev. D **88** 044004 (2013).

[15] Identification and mitigation of narrow spectral artifacts that degrade searches for persistent gravitational waves in the first two observing runs of Advanced LIGO, P. Covas *et al.*, Phys. Rev. D **97** 082002 (2018).

[16] See EPAPS Document No. [number will be inserted by publisher] for numerical values of upper limits.

[17] All-sky search for periodic gravitational waves in LIGO S4 data, B. Abbott *et al.* (LIGO Scientific Collaboration), Phys. Rev. D **77**, 022001 (2008).

[18] All-sky LIGO Search for Periodic Gravitational Waves in the Early S5 Data, B. P. Abbott *et al.* (LIGO Scientific Collaboration), Phys. Rev. Lett. **102**, 111102 (2009).

[19] All-sky Search for Periodic Gravitational Waves in the Full S5 Data, B. Abbott *et al.* (The LIGO and Virgo Scientific Collaboration), *Phys. Rev.* **D 85**, 022001 (2012).

[20] A Novel Universal Statistic for Computing Upper Limits in Ill-behaved Background, V. Dergachev, Phys. Rev. D **87**, 062001 (2013).

[21] Radio Pulsars in Terzan 5, A.G. Lyne *et al.*, M.N.R.A.S. **316** 491 (2000).

[22] Discovery of Three New Millisecond Pulsars in Terzan 5, M. Cadelano *et al.*, to appear in Astroph. J, arXiv:1801.09929, January 2018.

[23] R.N. Manchester, G.B. Hobbs, A. Teoh, M. Hobbs, AJ, 129, 1993-2006 (2005)

[24] B. P. Abbott *et al.* [LIGO Scientific and Virgo Collaborations], Phys. Rev. Lett. **116**, no. 6, 061102 (2016) doi:10.1103/PhysRevLett.116.061102 [arXiv:1602.03837 [gr-qc]].

[25] B. Behnke, M. A. Papa and R. Prix, Postprocessing methods used in the search for continuous gravitational-wave signals from the Galactic Center, Phys. Rev. D **91**, no. 6, 064007 (2015)

[26] C. Dreissigacker, R. Prix and K. Wette, Fast and Accurate Sensitivity Estimation for Continuous-Gravitational-Wave Searches, Phys. Rev. D **98**, no. 8, 084058 (2018)

[27] B. P. Abbott *et al.* [LIGO Scientific and Virgo Collaborations], Directional Limits on Persistent Gravitational Waves from Advanced LIGO First Observing Run, Phys. Rev. Lett. **118**, no. 12, 121102 (2017)

[28] B. P. Abbott *et al.* [LIGO Scientific and Virgo Collaborations], All-sky search for continous gravitational waves from isolated neutron stars using Advanced LIGO O2 data, arXiv:1903:01901